Journal of Engineering Physics and Thermophysics, Vol. 81, No. 5, 2008

MATHEMATICAL SIMULATION OF THE FORMATION OF HEAT TORNADOES

A. M. Grishin, O. V. Matvienko, and Yu. A. Rudi

UDC 621.1

A numerical simulation of convective swirling jets arising as a result of the rotation of a heated disk in an initially immovable medium has been carried out. It is shown that in the case where a jet is swirled moderately, the flow is relaminarized and the intensity of the heat and mass transfer in the convective jet decreases, which leads to an increase in the buoyancy force and, consequently, an increase in the velocity of the flow. The air mass in the form of a cylindrical column-shaped vortex rises above the disk to a large height and, in doing so, retains its individuality.

In [1], a complex investigation of free convective flows has been carried out. In [2], a review and a classification of different-type vortices and the theory of concentrated single vorticities, including tornadoes, are given. In [3], results of experimental investigations of tornado-like flows above a heated rotating disk in the atmosphere of an immovable air and a classification of the types of these flows are presented. One such flow is a tornado — a concentrated column-shaped vortex. In [4, 5], a theoretical model of formation of tornado-like vortices of an incompressible perfect liquid is proposed.

The heat transfer from the surface of a rotating disk has been investigated in [6]. In [7], some mechanisms of formation of heat and flame tornadoes have been determined experimentally. In [8, 9], a mathematical model of formation of a convective column and a flame tornado has been formulated for the case of forest fires and a mathematical simulation with this model has been performed.

The aim of the present work is to improve the mathematical model proposed in [3], to perform a numerical simulation of heat tornadoes arising as a result of the rotation of a heated disk in an initially immovable medium, and to substantiate this model by comparison of the numerical-simulation results with the experimental data of [3, 6, 7].

A scheme of physical simulation of the indicated vortices is given in [3, 7]. Disks of diameter D = 0.1–0.4 m were used in the investigations. The temperatures of the disks and the environment were assumed to be equal to T_* = 400–1000 K and T_e = 300 K, respectively.

Mathematical Model of a Heat Tornado. The problem is mathematically formulated with the following assumptions:

1) the flow in the region being considered is axisymmetrical;
2) the disk rotates with a constant angular velocity;
3) the power of the heat-release source does not change with time;
4) in the moving air there are regions of laminar, transient, and completely turbulent flows.

The characteristics of the flow and the heat transfer were calculated using the Reynolds equations of [10]. The characteristics of the turbulence were calculated with the use of the balance equations for the kinetic turbulent energy K and the rate of its dissipation ε with account for the action of the buoyancy forces, the smallness of the Reynolds numbers [11], the anisotropy of the turbulent pulsations [12], and the influence of the swirling on the stability of the turbulent flow [13]. The convection and the heat-transfer processes were defined with the heat-conduction equation. The density of the medium was determined by the equation of ideal-gas state. With allowance for the aforesaid we obtain the following system of equations:

Tomsk State University, 36 Lenin Ave., Tomsk, 634050, Russia; email: fire@mail.tsu.ru. Translated from Inzhenerno-Fizicheskii Zhurnal, Vol. 81, No. 5, pp. 860–867, September–October, 2008. Original article submitted September 26, 2007.

1062-0125/08/8105-0897

$$\frac{\partial \rho}{\partial t}+\frac{\partial \rho v_z}{\partial z}+\frac{1}{r}\frac{\partial \rho v_r r}{\partial r}=0\,, \tag{1}$$

$$\frac{\partial \rho v_z}{\partial t}+\frac{\partial \rho v_z^2}{\partial z}+\frac{1}{r}\frac{\partial \rho v_z v_r r}{\partial r}=-\frac{\partial p}{\partial z}+\frac{\partial}{\partial z}\left[\mu_{zz}\left(2\frac{\partial v_z}{\partial z}-\frac{2}{3}\left(\frac{\partial v_z}{\partial z}+\frac{1}{r}\frac{\partial v_r r}{\partial r}\right)\right)\right]+\frac{1}{r}\frac{\partial}{\partial r}\left[\mu_{zr} r\left(\frac{\partial v_z}{\partial r}+\frac{\partial v_r}{\partial z}\right)\right]-\rho g\,, \tag{2}$$

$$\frac{\partial \rho v_r}{\partial t}+\frac{\partial \rho v_z v_r}{\partial z}+\frac{1}{r}\frac{\partial \rho v_r^2 r}{\partial r}=-\frac{\partial p}{\partial r}+\frac{\partial}{\partial z}\left[\mu_{zr}\left(\frac{\partial v_r}{\partial z}+\frac{\partial v_z}{\partial r}\right)\right]$$

$$+\frac{1}{r}\frac{\partial}{\partial r}\left[\mu_{rr} r\left(2\frac{\partial v_r}{\partial r}-\frac{2}{3}\left(\frac{\partial v_z}{\partial z}+\frac{1}{r}\frac{\partial v_r r}{\partial r}\right)\right)\right]-\mu_{rr}\frac{v_r}{r}+\frac{\rho v_\varphi^2}{r}\,, \tag{3}$$

$$\frac{\partial \rho v_\varphi}{\partial t}+\frac{\partial \rho v_z v_\varphi}{\partial z}+\frac{1}{r}\frac{\partial \rho v_r v_\varphi r}{\partial r}=\frac{\partial}{\partial z}\left[\mu_{z\varphi}\frac{\partial v_z}{\partial z}\right]+\frac{1}{r^2}\frac{\partial}{\partial r}\left[\mu_{r\varphi} r^3\frac{\partial}{\partial r}\left(\frac{v_z}{r}\right)\right]-\frac{\rho v_r v_\varphi}{r}\,, \tag{4}$$

$$\frac{\partial \rho k}{\partial t}+\frac{\partial \rho k}{\partial z}+\frac{1}{r}\frac{\partial \rho v k r}{\partial r}=\frac{\partial}{\partial z}\left[\frac{\mu}{\sigma_k}\frac{\partial k}{\partial z}\right]+\frac{1}{r}\frac{\partial}{\partial r}\left[\frac{\mu}{\sigma_k} r\frac{\partial k}{\partial r}\right]+G_k+P-D-\rho\varepsilon\,, \tag{5}$$

$$\frac{\partial \rho \varepsilon}{\partial t}+\frac{\partial \rho \varepsilon}{\partial z}+\frac{1}{r}\frac{\partial \rho v \varepsilon r}{\partial r}=\frac{\partial}{\partial z}\left[\frac{\mu}{\sigma_\varepsilon}\frac{\partial \varepsilon}{\partial z}\right]+\frac{1}{r}\frac{\partial}{\partial r}\left[\frac{\mu}{\sigma_\varepsilon}\frac{\partial \varepsilon}{\partial r}\right]$$

$$+\left(C_{1\varepsilon}\left(G_k+C_{3\varepsilon}\max(0,P)+C_1' w\frac{\partial}{\partial r}\left(\frac{v_\varphi}{r}\right)\right)-C_{2\varepsilon} f_{2\varepsilon}\rho\varepsilon\left(1-C_2'\frac{k^2}{\varepsilon^2}\frac{v_\varphi}{r^2}\frac{\partial v_\varphi r}{\partial r}\right)\right)\frac{\varepsilon}{k}+E\,, \tag{6}$$

$$c_p\left(\frac{\partial \rho T}{\partial t}+\frac{\partial \rho v_z T}{\partial z}+\frac{1}{r}\frac{\partial \rho_r v T}{\partial r}\right)=\frac{\partial}{\partial z}\left[\lambda_{zz}\frac{\partial T}{\partial z}\right]+\frac{1}{r}\frac{\partial}{\partial r}\left[\lambda_{rr} r\frac{\partial T}{\partial r}\right], \tag{7}$$

$$\rho=\frac{pM}{R_* T}\,, \tag{8}$$

$$\mu_{ij}=\mu_0+K_{ij}\mu_t\,,\quad \lambda_{ij}=\lambda_0+c_p K_{ij}\mu_t/\mathrm{Pr_t}\qquad (ij = zz, zr, z\varphi, rr, r\varphi, \varphi\varphi)\,,$$

$$K_{ij}=\begin{pmatrix}1.04 & 0.01 & 1\\ 0.01 & 0.1 & 0.025\\ 1 & 0.025 & 1\end{pmatrix},\quad \mu_t=C_\mu f_\mu \rho\frac{k^2}{\varepsilon}\,,$$

$$G_k=\mu_t\left\{2\left[\left(\frac{\partial v_z}{\partial z}\right)^2+\left(\frac{\partial v_r}{\partial r}\right)^2+\left(\frac{v_r}{r}\right)^2\right]+\left(\frac{\partial v_z}{\partial r}\right)^2+\left(\frac{\partial v_r}{\partial z}\right)^2+\left(\frac{\partial v_\varphi}{\partial z}\right)^2+\left(r\frac{\partial}{\partial r}\left(\frac{v_\varphi}{r}\right)\right)^2\right\},$$

$$P=-\frac{\mu_{zz}}{\rho\sigma}\mathbf{g}\cdot\mathrm{grad}\,(\rho)\,,\quad D=2\mu_0\,(\mathrm{grad}\,\sqrt{k})^2\,,\quad E=2\frac{\mu\mu_t}{\rho}\left[\mathrm{div}\,(\mathrm{grad}\,(\mathbf{v}))\right]^2,$$

$$f_\mu = \exp\left[-\frac{3.4}{(t+\mathrm{Re_t}/50)^2}\right],\ f_2 = 1 - 0.3\exp\left(-\mathrm{Re_t}^2\right),\ \mathrm{Re_t} = \frac{\rho k^2}{\mu\varepsilon}.$$

To the constants involved in the equations we were given the values recommended in [13]: $C_{1\varepsilon}$ = 1.44, $C_{2\varepsilon}$ = 1.92, C_1' = 0.9, C_2' = 0.2, $C_{3\varepsilon}$ = 0.8, σ_ε = 1.3, σ_k = 1, C_μ = 0.09, $\mathrm{Pr_t}$ = 0.7. The values of the physical parameters — the viscosity, heat conduction, and heat capacity of the flow — were determined for different temperatures in accordance with the data presented in [14].

The system of equations (1)–(8) was solved for the following initial and boundary conditions:

$$t = 0:\ v_z = 0,\ v_r = 0,\ v_\varphi = 0,\ k = 0,\ \varepsilon = 0,\ T = T_{\mathrm{in}}; \tag{9}$$

at $t > 0$, at the boundaries of the computational region the following conditions were fulfilled:

$$z = 0,\ r \le D/2:\ v_z = 0,\ v_r = 0,\ v_\varphi = \omega r,\ k = \mathrm{Tu}\, v_\varphi^2,\ T = T_*; \tag{10}$$

$$z = 0,\ r > D/2:\ v_z = 0,\ v_r = 0,\ v_\varphi = 0,\ T = T_{\mathrm{e}}; \tag{11}$$

$$r = 0:\ \frac{\partial v_z}{\partial r} = 0,\ v_r = 0,\ v_\varphi = 0,\ \frac{\partial T}{\partial r} = 0,\ \frac{\partial k}{\partial r} = 0,\ \frac{\partial \varepsilon}{\partial r} = 0; \tag{12}$$

$$r = R_\infty:\ v_z = 0,\ v_\varphi = 0,\ \frac{\partial r v_r}{\partial r} = 0,\ \frac{\partial T}{\partial r} = 0,\ \frac{\partial k}{\partial r} = 0,\ \frac{\partial \varepsilon}{\partial r} = 0; \tag{13}$$

$$z = H_\infty:\ \frac{\partial v_z}{\partial z} = 0,\ \frac{\partial v_\varphi}{\partial z} = 0,\ v_r = 0,\ \frac{\partial T}{\partial z} = 0,\ \frac{\partial k}{\partial z} = 0,\ \frac{\partial \varepsilon}{\partial z} = 0. \tag{14}$$

In Eqs. (13) and (14), R_∞ and H_∞ are computational parameters assumed to be equal to 2 and 10 m, respectively, and Tu is a parameter characterizing the initial turbulence of the flow. In the main calculations, Tu = 0.03.

Methods of Solution. The above-considered equations were solved numerically with the use of the finite-volume method. In accordance with this method, the finite-difference equations are obtained by integration of differential equations with respect to control volumes containing nodes of a finite-difference grid. The numerical solution was carried out on a staggered grid, and the nodes for the axial and radial velocity components were located at the center of the faces of the control volumes for scalar quantities. The calculations were carried out on a grid with 210 nodes in the axial direction and 176 nodes in the radial one.

For estimation of the accuracy of calculations, we carried out a series of calculations with the use of sequences of bunching grids. The results of the testing show that a decrease in the pitch of the base grid, on which the main calculations were performed, along the axial and radial coordinates by two times changes the values of the main variables by no more than 3%. The convective terms were approximated using the upwind QUICK scheme of the third order of accuracy, proposed by Leonard [15], and the diffusion terms were approximated using the central-difference scheme. The continuity equation was satisfied indirectly with the use of the SIMPLEC algorithm [16]. The system of nonlinear algebraic equations was solved numerically with the use of iterations. It was assumed that the iterative convergence is attained if the mean-square discrepancy for all the variables does not exceed 1%.

Analysis of Results. The main characteristic movement of a nonrotating disk in the convection regime causes a rise of the heated air above the disk and, as a result, a sideward motion of the air at the disk edges. At the initial stage of this motion, the air flows from the peripheral region of the disk to its heated horizontal region. In this case, the intensity of the radial flow is determined by the power of the heat source. An upward flow in the form of a stationary torch is formed above the surface of the disk.

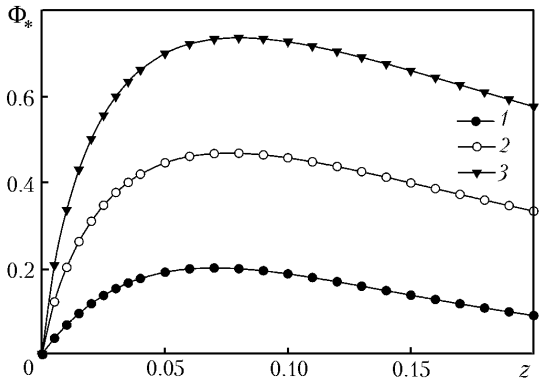

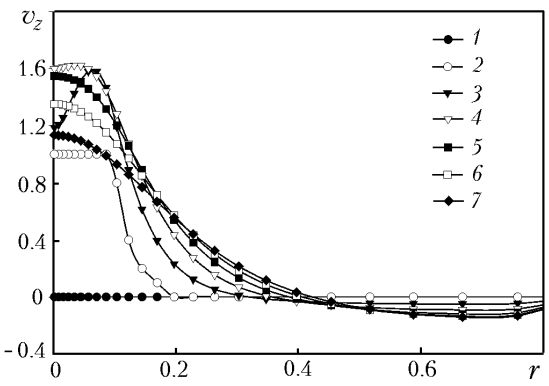

Fig. 1. Change in the Heeger–Beer parameter with height: ω = 0.5 (1), 1.5 (2), and 2 sec^{-1} (3). z, m.

Fig. 2. Radial distribution of the axial velocity: x = 0 (1), 5 (2), 15 (3), 25 (4), 30 (5), 35 (6), and 40 cm (7). ω = 1.5 sec^{-1}, T_{in} = 300 K, T_* = 450 K. v_z, m/sec; r, m.

In the main region of the jet, the buoyancy force dominates, with the result that the velocity of the flow increases. As the flow cools down, the role of the buoyancy force decreases and becomes negligibly small; in this case, the air flows by inertia and, in doing so, decelerates gradually as a result of the action of the viscous forces. Therefore, this region of the jet can be considered as inertial. The air mass forming the torch is mixed with the environmental air. The stationary torch is scattered gradually and disappears.

The swirling of the gas flow leads to the appearance of the tangential component of the velocity w and the formation of the field of centrifugal forces; these forces are proportional to $\rho w^2/r$ and intensify the gas motion in the radial direction. The influence of the swirling of the jet on the structure of the flow and the heat transfer in it is conveniently characterized by the integral Heeger–Beer parameter of swirling [10], representing the ratio between the axial component of the angular moment of the flow and the product of the radius of the channel by the axial component of this moment:

$$\Phi_* = \frac{2\int\limits_0^R \rho v_z v_\varphi r^2 dr}{D\int\limits_0^R \rho\left[v_z^2 + (p+\rho g z)\right] r dr}. \qquad (15)$$

The change in the parameter Φ_* with height is shown in Fig. 1. As is seen from this figure, the Heeger–Beer parameter increases in the initial region of the jet, which is explained by the entrainment of the air mass sucked from the peripheral region into the rotation. Then, downstream, as the swirling of the jet degenerates, Φ_* decreases. An increase in the rotational velocity of the disk leads to an increase in the swirling of the jet; in this case, a maximum of Φ_* is attained at a smaller distance from the disk. A weak swirling ($\Phi_* < 0.3$) practically has no influence on the pattern of the flow. However, when the swirling of the jet increases, in its central near-axis region there appear zones with a rarefaction or a smaller static pressure due to the centrifugal effect. Because of this, dips arise in the profile of the transverse axial velocity of the flow in the near-axis zone of the jet when its swirling is moderate ($0.3 < \Phi_* < 0.6$) and back currents arise in the case of strong swirling of the jet ($\Phi_* > 0.6$).

Figure 2 shows radial distributions of the axial velocity of the flow at different heights of a jet with moderate swirling. Near the surface of the disk, in the region where the swirling of the jet is fairly small, the distribution of the axial velocity of the flow is monotonic. Then, as the swirling of the jet increases, the curve $v_z(r)$ takes a characteristic form with a displacement of the maximum relative to the center and a dip at the center. When the distance between the flow and the disk increases further, the width of the jet increases, the inner zone with a velocity dip disappears, and the velocity profile deforms and becomes monotonic.

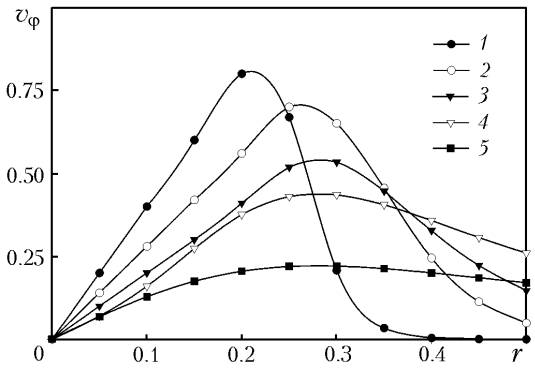

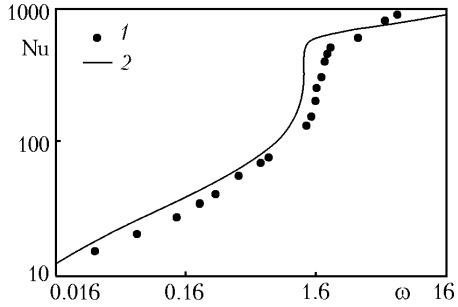

Fig. 3. Radial distribution of the tangential velocity: x = 5 (1), 10 (2), 15 (3), 20 (4), and 25 cm (5). T_{in} = 300 K, T_* = 450 K. v_φ, m/sec; r, m.

Fig. 4. Change in the intensity of the heat transfer from a rotating disk: 1) experiment [3]; calculation (2). ω, sec^{-1}.

The radial distribution of the tangential velocity of the flow in a jet formed above a heated disk is shown in Fig. 3. This jet contains a central core rotating quasi-rigidly and an outer region rotating quasi-potentially. Outside the central region, the conditions for a free vortex are prevailing. Thus, the rotation of the flow being considered can be described with the use of a free forced vortex, which, as applied to the atmospheric phenomena, corresponds to the formation of tornadoes, dust storms, and other tornado-like vortices.

In the above-described jet there are three regions, in which the change from the laminar to the turbulent regime of flow is realized, and regions where the flow is laminarized. Near the surface of the disk, in the heated boundary layer, there arises a laminar flow that is transformed into the turbulent one in the main region of the jet. It should be noted that, in this case, a laminar flow can be formed at the periphery of the jet stream. In the inertial region of the jet, where the velocity of the rising air flow increases, the intensity of the turbulent pulsations decreases and the flow relaminarizes.

The swirling of the jet influences not only the structure of the flow, but also the characteristics of its turbulence. One mechanism of this influence is fairly evident. A swirling of the flow gives rise to large gradients of the velocity of the flow and, in doing so, generates turbulent stresses. In a swirling jet, the influence of the centrifugal force on the structure of the flow is similar in character to the action of the temperature stratification in the field of a gravity force [17]. In this case, depending on the character of the radial distribution of the velocity components, the kinetic energy can be transformed into the potential one — a conservative action or, conversely, an active action. The centrifugal force aids in increasing turbulent pulsations in the case of an active action and suppresses these pulsations in the case of a conservative action.

The action of the swirling of a jet on the turbulence of the flow is defined by the terms accounting for the influence of the swirling on the dissipation of the turbulent energy, added into the equation for the rate of dissipation of the turbulent energy ε (6):

$$C_{1\varepsilon}C_1' w \frac{\varepsilon}{k}\frac{\partial}{\partial r}\left(\frac{v_\varphi}{r}\right) + C_2' C_{2\varepsilon} f_{2\varepsilon} \rho\varepsilon \frac{k}{\varepsilon}\frac{v_\varphi}{r^2}\frac{\partial v_\varphi r}{\partial r}.$$

Analysis of these terms with consideration for the radial distribution of the tangential velocity of the flow (see Fig. 3) allows the conclusion that the swirling of a jet exerts a conservative or, at least, a neutral action on its turbulent pulsations, which is most marked in jets with a moderate swirling. This effect does not arise in jets with a weak swirling because of the smallness of the indicated action in them. In jets with a strong swirling, the influence of the swirling on the turbulence plays a dominant role, which is explained by the appearance of large gradients of the velocity of the average flow and, as a consequence, the increase in the turbulent stresses.

Thus, the structure of the turbulence in a jet with a moderate swirling is characterized by an intensive turbulization in the vicinity of the surface of the disk and a not less intensive relaminarization in the main region of the flow.

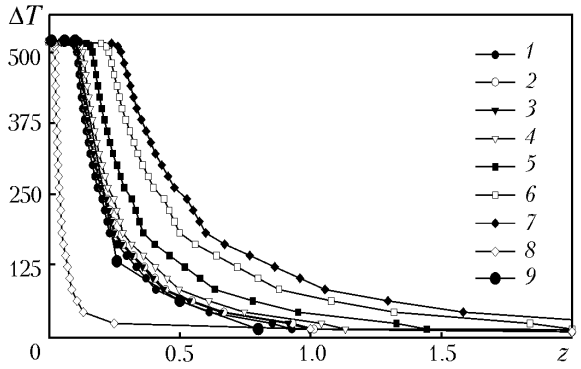

Fig. 5. Change in the temperature at the axis of the flow: ω = 0 (1), 0.15 (2), 0.33 (3), 0.75 (4), 1 (5), 1.25 (6), 1.5 (7), 2 (8), and 0.33 sec^{-1} (9) (experiment). ΔT, K; z, m.

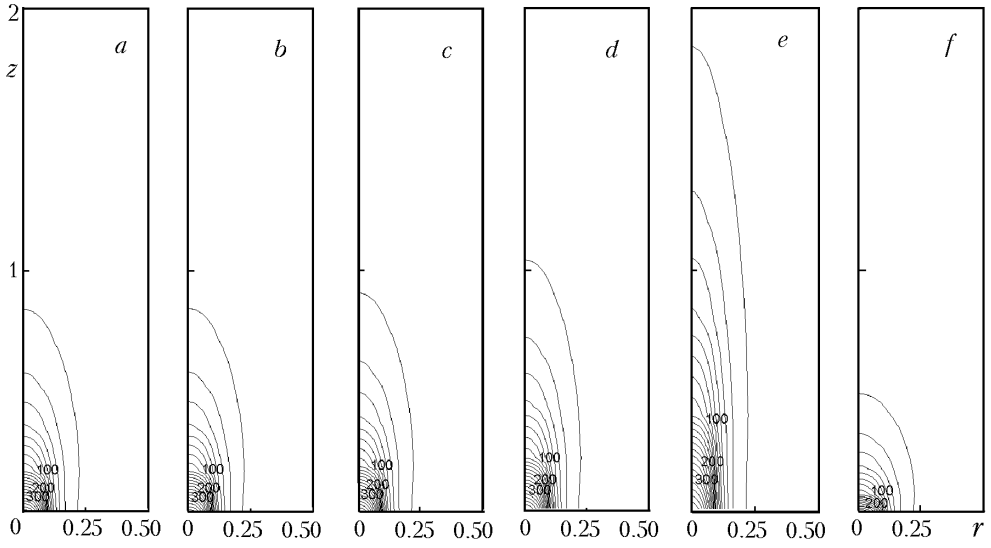

Fig. 6. Distribution of isotherms in the flow (the minimal isotherm corresponds to the temperature 50°C, the spacing between the isolines is equal to 20°C): ω = 0 (a), 0.15 (b), 0.5 (c), 1 (d), 1.5 (e), and 2 sec^{-1} (f). z, r, m.

Figure 4 shows a comparison of the Nusselt numbers $Nu = \alpha D/\lambda_0$, calculated on the basis of the turbulence model adopted here, with the experimental data of [6], characterizing the heat transfer from a rotating disk. As is seen from this figure, the heat-transfer coefficient characterized by the parameter Nu increases with increase in the angular rotational velocity of the disk. In this case, the change to the turbulent regime of heat transfer is accompanied by a sharp increase in the heat transfer from the surface of the disk. The results of the calculations are in satisfactory agreement with the experimental data throughout the range of swirlings being investigated. A small deviation of the calculation data from the experimental ones is probably due to the more complex mechanism of decreasing the stability of the jet and the appearance of a turbulence.

The change in the excess temperature $\Delta T = T - T_e$ at the axis of a jet is shown in Fig. 5. The results obtained are in satisfactory qualitative agreement with the experimental data [3] (the comparison is given for the maximum temperature difference). The small difference between the calculation and experimental data near the surface of the disk can be explained by the features of the installation of the disk on the test bed that were not taken into account in the theoretical investigation.

It is seen from Fig. 5 that the temperature distribution along the axis of the flow has two regions. In the first, initial region, the temperature remains practically unchanged, and, in the second region, the temperature decreases ex-

ponentially. An increase in the angular rotational velocity of the disk to $\omega < 1.5$ sec^{-1} leads to an increase in the temperature of the flow and to an elongation of the region with a nearly constant temperature distribution. The temperature of the flow decreases fairly abruptly when its swirling increases.

The reasons for such behavior of the temperature of the flow being considered are the features of its turbulent structure. An increase in the rotational velocity of the disk to $\omega < 1.5$ sec^{-1} leads to an intensification of the heat exchange between the air and the heater (because of the turbulization of the flow in the main region of the jet). A decrease in the heat exchange with the environmental air leads to an increase in the buoyancy force and, consequently, an increase in the velocity of the flow. When the angular rotational velocity of the disk falls within the range 1 sec^{-1} $< \omega <$ 1.5 sec^{-1}, the air mass shaped as a laminarized cylinder rises to a large height and, in doing so, retains its individuality (Fig. 6a–e). A flow of this type can be considered as the initial stage of formation of a heat tornado (Fig. 6e).

Our calculations have shown that a heat tornado can exist in the narrow range of angular rotational velocities of a disk 1 sec^{-1} $< \omega <$ 1.5 sec^{-1}. At $\omega > 1.5$ sec^{-1} the jet breaks down and the height of the swirling convective column decreases markedly (Fig. 6f).

Analytical Formula for the Height of a Heat Tornado. An analysis of the experimental and theoretical investigations [3–6] allows the conclusion that the determining condition for the formation of a heat tornado is the existence of a local equilibrium between the acting forces. If the assumption is made that the heat energy supplied to the tornado is completely transformed into the potential one, the height of the heat tornado can be determined by the formula

$$h = \frac{1}{2g}\left(\frac{Q}{\rho T_* D^2}\right)^{2/3} \frac{T_e}{T_* - T_e}. \tag{16}$$

Here Q is the intensity of heating of the air mass by a rotating disk. In accordance with [4], this energy can be determined as

$$Q = \left(3.6 + 0.1\mathrm{Re}_\omega^{0.6}\right)\lambda D\,(T_* - T_e), \tag{17}$$

where $\mathrm{Re}_\omega = \rho\omega\pi D^2/2\mu$ is the Reynolds number of the rotational motion.

The results of calculations by formula (16) with the use of (17) give the overstated value of the height of a heat tornado because these formulas take no account for the heat losses caused by the heating of the environmental air. Therefore, formula (16) should be corrected with allowance for the heat exchange. The heat energy expended for the rise of the air mass can be determined from the formula

$$Q_* = f(\mathrm{Re}_\omega)\, Q,$$

where $f(\mathrm{Re}_\omega)$ is the function of the Reynolds number of the rotational motion, characterizing the heat losses. The processing of the calculation data has shown that the following dependence can be used:

$$f(\mathrm{Re}_\omega) = 0.6 \cdot \exp\left(-0.002\,\mathrm{Re}_\omega^{0.6}\right).$$

The finite formula for determining the height of a heat tornado has the form

$$h = \frac{1}{2g}\left(\frac{f(\mathrm{Re}_\omega)\, Q}{\rho T_* D^2}\right)^{2/3} \frac{T_e}{T_* - T_e}.$$

Thus, in the case of a moderate swirling of a jet a heat tornado arises as a result of the formation of a local equilibrium in a free forced vortex due to the anisotropy of the turbulence of the flow and its laminarization leading to a decrease in the heat exchange with the ambient air and, consequently, to an increase in the buoyancy force and an increase in the velocity of the flow.

This work was carried out with financial support from the Russian Foundation for Basic Research No. 08-01-00496.

NOTATION

c_p, specific heat capacity at a constant pressure, J/(kg·K); D, diameter of a disk, m; g, free fall acceleration, m/sec^2; h, height of a heat tornado, m; k, kinetic turbulent energy, J/kg; M, molecular mass of a gas, kg/mole; Nu, Nusselt number; p, dynamic pressure, Pa; Pr, Prandtl number; Q, intensity of heating of air masses by the rotating disk, W; R_*, universal gas constant, J/(mole·K); r, radial coordinate, m; Re_ω, Reynolds number of the rotational motion; Tu, intensity of the turbulence of a flow; T, temperature, K; $\mathbf{v}$, velocity vector; v_z, v_r, and v_φ, axial, radial, and tangential velocity components, m/sec; z, axial coordinate, m; α, heat-transfer coefficient, W/(m^2·K); ε, rate of dissipation of the turbulent energy, W/kg; λ, heat-conductivity coefficient, W/(m·K); μ, dynamic viscosity, Pa·sec; ρ, density, kg/m^3; ω, angular rotational velocity of the disk, 1/sec; Φ_*, Heeger–Beer parameter of swirling. Subscripts: e, environment; in, input parameters; t, turbulent; 0, molecular; ∞, parameters at infinity.

REFERENCES

1. B. Gebhart, Y. Jaluria, R. L. Mahajan, and S. Sammaki, *Buoyancy-Induced Flows and Transport* [Russian translation], Mir, Moscow (1991).
2. S. V. Alekseenko, P. A. Kuibin, and V. L. Okulov, *Introduction to the Theory of Concentrated Vortices* [in Russian], ITF SO RAN, Novosibirsk (2003).
3. B. M. Bubnov, Thermal structure and turbulization of tornado-like vortices from localized heat sources above a rotating disk, *Izv. Akad. Nauk SSSR*, *Fiz. Atmos. Okeana*, **33**, No. 4, 434–442 (1977).
4. V. V. Nikulin, Investigation of the interaction of a tornado-like vortex with solid boundaries, *Prikl. Mekh. Tekh. Fiz.*, No. 1, 68–75 (1980).
5. V. V. Nikulin, An analog of the equations of eddy shallow water for hollow and tornado-like vortices. The height of a stationary tornado-like vortex, *Prikl. Mekh. Tekh. Fiz.*, No. 2, 45–51 (1992).
6. Cz. O. Popiel and L. Boguslawski, Local heat transfer coefficients on the rotation disc in still air, *Int. J. Heat Mass Transfer*, **18**, 167–173 (1975).
7. A. M. Grishin, A. N. Golovanov, and Ya. V. Sukov, Physical simulation of flame tornadoes, *Dokl. Ross. Akad. Nauk*, **395**, No. 2, 196–198 (1975).
8. A. M. Grishin and O. V. Matvienko, Mathematical simulation of flame tornadoes, in: *Heat- and Mass Transfer–MIF-2004*, *5th Minsk Int. Forum*, 24–28 May, 2004, Minsk (2004), pp. 174–176.
9. A. M. Grishin and O. V. Matvienko, Mathematical simulation of the dynamics of formation of a convective column and a flame tornado in forest fires, in: *Proc. 13th Symp. on Combustion and Explosion*, January 7–11, 2005, Chernogolovka.
10. A. K. Gupta, D. G. Lilley, and N. Syred, *Swirl Flows* [Russian translation], Mir, Moscow (1987).
11. M. A. Leschziner and W. Rodi, Computation of strongly swirling axisymmetric free jets, *AIAA J.*, **22**, No. 11, 370–373 (1984).
12. T. Kobayashi and M. Yoda, Modified k–ε model for turbulent swirling flow in a straight pipe, *JSME Int. J.*, **30**, 66–71 (1987).
13. J. Piquet, *Turbulent Flows: Models and Physics*, Springer, Berlin (1999).
14. T. Cebeci and P. Bradshaw, *Physical and Computational Aspects of Convective Heat Transfer* [Russian translation], Mir, Moscow (1987).
15. B. P. Leonard, A stable and accurate convection modeling procedure based on quadratic upstream interpolation, *Comput. Meth. Appl. Mech. Eng.*, **19**, 59–98 (1979).
16. J. P. Van Doormal and G. D. Raithby, Enhancements of the SIMPLE method for predicting incompressible fluid flows, *Numer. Heat Transfer*, **7**, 147–163 (1984).
17. A. A. Khalatov, *Theory and Practice of Swirling Flows* [in Russian], Naukova Dumka, Kiev (1989).